

Article

Not peer-reviewed version

# First-Principle Prediction of Stress-Tunable Single-Photon Emitters at Telecommunication Band from Point Defects in GaN

Junxiao Yuan <sup>#</sup>, Ke Wang <sup>#</sup>, [Yidong Hou](#), [Feiliang Chen](#) <sup>\*</sup>, [Qian Li](#) <sup>\*</sup>

Posted Date: 21 March 2023

doi: 10.20944/preprints202303.0362.v1

Keywords: single-photon emitters; atom defect; first principle calculations; telecommunication band; stress



Preprints.org is a free multidiscipline platform providing preprint service that is dedicated to making early versions of research outputs permanently available and citable. Preprints posted at Preprints.org appear in Web of Science, Crossref, Google Scholar, Scilit, Europe PMC.

Copyright: This is an open access article distributed under the Creative Commons Attribution License which permits unrestricted use, distribution, and reproduction in any medium, provided the original work is properly cited.

## Article

# First-Principle Prediction of Stress-Tunable Single-Photon Emitters at Telecommunication Band from Point Defects in GaN

Junxiao Yuan <sup>1,†</sup>, Ke Wang <sup>1,†</sup>, Yidong Hou <sup>1</sup>, Feiliang Chen <sup>2,\*</sup> and Qian Li <sup>3,\*</sup>

<sup>1</sup> Department of Physics, Sichuan University, Sichuan, 610065, China

<sup>2</sup> School of Electronic Science and Engineering, University of Electronic Science and Technology of China, Chengdu, 610054, China

<sup>3</sup> Microsystem and Terahertz Research Center, China Academy of Engineering Physics, Chengdu, 610299, China

\* Correspondence: flchen@uestc.edu.cn (F.C.); liqian\_mtrc@caep.cn (Q.L.)

† J. Yuan and Ke Wang contributed equally to this work.

**Abstract:** Point defect-based single-photon emitters (SPEs) in GaN have aroused a great deal of interest due to their room-temperature operation, narrow line width and high emission rate. The room-temperature SPEs at the telecommunication bands have also been realized recently by localized defects in GaN in experiments, which are highly desired for the practical applications of SPEs in quantum communication with fiber compatibility. However, the origin and underlying mechanism of the SPEs remain unclear to date. Herein, our first-principle calculations predict and identify an intrinsic point defect  $N_{Ga}$  in GaN that owns a zero-phonon line (ZPL) at telecommunication windows. By tuning the triaxial compressive strain of the crystal structure, the ZPL of  $N_{Ga}$  can be modulated from 0.849 eV to 0.984 eV, covering the fiber telecommunication windows from the O band to the E band. Besides the ZPL, the formation energy, band structure, transition process and lifetime of the SPEs under different strains are investigated systematically. Our work gives insight into the emission mechanism of the defect SPEs in GaN and also provides effective guidance for achieving wavelength-tunable SPEs working in fiber telecommunication windows.

**Keywords:** single-photon emitters; atom defect; first principle calculations; telecommunication band; stress

## 1. Introduction

As a central building block for quantum information technologies, single-photon emitters (SPEs) could be widely used in quantum secure communication, optical quantum computing and so on [1–3]. An isolated two-level quantum system composed of an excited state and a ground state is necessary for an ideal SPE, where the electron only prefers to transit in this two-level quantum system through absorbing or emitting one photon at a time [4]. In recent years, point defects in wide bandgap semiconductor have been widely demonstrated as one of the best choices to realize the room temperature (RT) SPEs. Electron wave functions of point defects localized at the atomic scales contribute to the formation of defect levels which could make up isolated and heat-stabilized two-level system. However, the practical applications of SPEs on quantum communication require data transmission over optical fibers, and most of the RTSPEs are located in visible wavelengths so far, where the attenuation of photons in fiber is more than 3 dB/km and unsuitable for long distance transmission [5]. On the other hand, the fiber telecommunication windows (from 1260 nm to 1675 nm, or from O to U band) at near infrared (NIR) are widely used in fiber-based long-distance telecommunications, benefiting from the low attenuation (0.3 dB/km for 1310nm and 0.15 dB/km for 1550 nm). In the meanwhile, the solar radiation and Rayleigh scattering in the NIR fiber windows are also relatively low, and the free-space telecommunication is also applicable in this waveband. Therefore, RT SPEs working in fiber telecommunication windows need to be exploited.

GaN is the most commercialized III-nitride materials and has been developed to realize SPEs based on the localized point defects inside [6,7]. Its wide direct bandgap [8] can suppress the interaction between the defect levels in band gap and the bulk states, while the weak photoacoustic coupling could produce a zero-phonon line (ZPL) with narrow line width. The RT defect SPEs in GaN were firstly realized in experiment by Berhane et al. in 2017 and the measured ZPL varied from 620 nm to 780 nm [9]. Then in 2018, high-performance RT SPEs in the telecom range (about 1000 nm - 1300 nm) were further found in GaN [10], but their origin and defect atom structure are still unclear. As for theory, although the calculations of Zang et al. indicated that neutral  $V_{Ga}$  can work as a potential SPE working in NIR and its ZPL can be tuned by the strain [11], the requirement of a specific p-type GaN to maintain its neutral state does not agree well with the experiment results. Therefore, much more effort should be paid to exploring the possible origin and emission mechanism of the defect SPEs in GaN operating in the fiber telecommunication band.

On the other hand, the influence of strain on SPEs has attracted wide interest recently, which can effectively modify emission properties such as wavelength and polarization. Gabriele's work has confirmed the non-monotonic behavior of the ZPL energy in hexagonal boron nitride under the effect of strain, and its role in the large spectral distribution was also observed experimentally [12]. This modulation effect of strain on ZPL wavelength provides a possible way to explain the emission in the fiber telecommunication band for SPEs in GaN, and also inspire new applications, such as the multidimensional information coding.

In this work, we carried out a systematic theoretical analysis on the intrinsic atom defects in GaN through first principle calculation and find a point defect  $N_{Ga}$  that can produce SPE with ZPL in the fiber telecommunication band. By tuning the triaxial compressive strain of the crystal structure, the ZPL could be adjusted from the O band to the E band (1260 nm to 1460 nm). The formation energy, band structure, charge density, transition mechanism, and orbital composition of the point defect  $N_{Ga}$  in GaN have been systematically investigated.

## 2. Calculation Methods

Our first principle calculations based the density functional theory (DFT) were performed by the PWmat package [13,14]. The atomic positions of the defect structure were optimized with the Perdew-Burke-Ernzerhof (PBE) functional [15], and the self-consistent field (SCF) calculations to give the band structure were performed with the Heyd-Scuseria-Ernzerhof (HSE) hybrid functional [16]. All calculations were spin-polarized, and the energy cutoff for the basis function was set to 70 Ry (Rydberg). Since strain calculation involving cell size change required higher calculating accuracy than the formation calculation, the k-point set mesh parameter in strain relaxation calculation was set to  $3 \times 3 \times 3$  while the mesh parameter in formation calculation was set to  $3 \times 3 \times 2$ .

The bulk GaN has a typical wurtzite structure with space group  $P6_3mc$ . The defect calculations are carried out with a supercell consisting of  $3 \times 3 \times 2$  primitive cells, as shown in Figure 1. The triaxial strain  $\sigma < 1$  represents the compressive strain, while  $\sigma > 1$  represents the tensile strain. The lattice constant parameters corresponding to the supercell with  $\sigma=1$  are  $a = b = 9.504 \text{ \AA}$ ,  $c = 10.323 \text{ \AA}$ ,  $\alpha = \beta = 90^\circ$ , and  $\gamma = 120^\circ$ . The defect model  $N_{Ga}$  ( $GaN$ ) used in this article is the GaN supercell in which a Ga (or N) atom is replaced by an N (or Ga) atom.

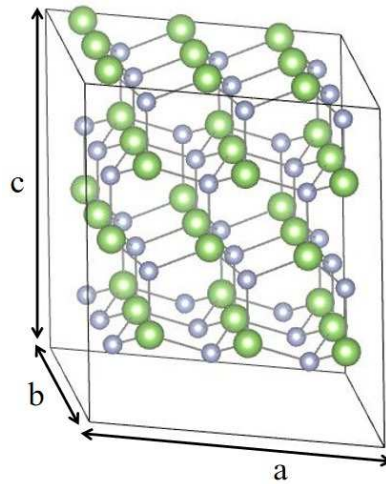


**Figure 1.** Supercell structure of the GaN crystal.

### 3. Results

#### 3.1. Formation Energy and Thermodynamic Stability of Single-Atom Defects

In our previous work [17], we demonstrated that defects  $V_N$  and  $N_i$  can be easily formed in experiments due to their low formation energy. However, their high concentration leads to the formation of a luminescence band rather than a stable single photon emitter (SPE), as the defects become too close to each other and become indistinguishable in space. In GaN,  $V_N$  has been confirmed to cause a green luminescence band [18], while  $N_i$  causes a yellow luminescence band [19]. On the other hand,  $Ga_i$  has a high formation energy in N rich conditions, which lead to small concentration. Although its low migration energy reported in Ref [20] suggests that it cannot serve as a stable SPE as it easily diffuses in GaN. Neutral  $V_{Ga}$ , with a high formation energy in both N rich (7.9 eV) and Ga rich (6.7 eV) conditions, has the potential to serve as an SPE, as suggested by the calculation results from Zang et al [11]. However, its 5-electron-8-orbital electronic configuration is only stable in the lower part of the band gap according to the formation energy diagram. This indicates that a specific p-type GaN is required to maintain its neutral state, which is challenge to be realized in experiment. In terms of intrinsic point defects,  $Ga_N$  and  $N_{Ga}$  are the only possible defects that can serve as SPEs in telecommunication windows. Therefore, we focus our discussion on  $Ga_N$  and  $N_{Ga}$ . Their thermodynamic stability is assessed by calculating their formation energies, which are as follows:

$$E_f(\alpha, q, E_F) = E_{tot}(\alpha, q) - E_{tot}(\text{host}) + \sum n_i \mu_i + q(E_F + E_{VBM}(\text{host})) + E_{corr} \quad (1)$$

Where  $E_{tot}(\alpha, q)$  is the total energy of the supercell with defect  $\alpha$  in charge state  $q$ , and  $E_{tot}(\text{host})$  is the total energy of the same supercell without defect.  $\sum n_i \mu_i$  is the chemical potential of atom  $i$ , and  $n_i$  is the number of element  $i$  removed from the cell to form defect  $\alpha$ .  $E_{VBM}(\text{host})$  is the eigenvalue of the valence band maximum (VBM) level aligned with reference to the electrostatic potential far from the defect site in the supercell and  $E_F$  is the Fermi level referring to the VBM level. A high Fermi level usually requires a high electron concentration, i.e., a n-type environment.  $E_{corr}$  is a corrected value caused by the long-range image-charge Coulomb interaction [21].

Formula (1) shows that the line slope for formation energy  $E_f(\alpha, q, E_F)$  is charge  $q$ . As seen in Figure 2, it is evident that among their own charged states, the neutral  $N_{Ga}$  and neutral  $Ga_N$  have the highest formation energy among their own charged states. The neutral  $N_{Ga}$  can remain stable at a Fermi energy ranging from 1.7 eV to 2.6 eV (marked in red shadow), which is corresponding to a weak n-type doping environment for unintentional doping in GaN. On the other hand,  $Ga_N$  requires a stronger n-type doping environment than  $N_{Ga}$  and can remain stable at a Fermi energy ranging from 2.3 eV to 3.0 eV (marked in gray shadow). The  $N_{Ga}^{1.005}$  and  $N_{Ga}^{0.995}$  are the 0 state  $N_{Ga}$  with  $\sigma=100.5\%$  and  $\sigma=99.5\%$ , respectively.  $N_{Ga}^{0.995}$  is shifted up by 0.15 eV compared to  $\sigma=100\%$ , while  $N_{Ga}^{1.005}$  is

shifted down by 0.03 eV. Despite these minor shifts, it is evident that the formation energy and stability of these defects would not be significantly affected by these strains.

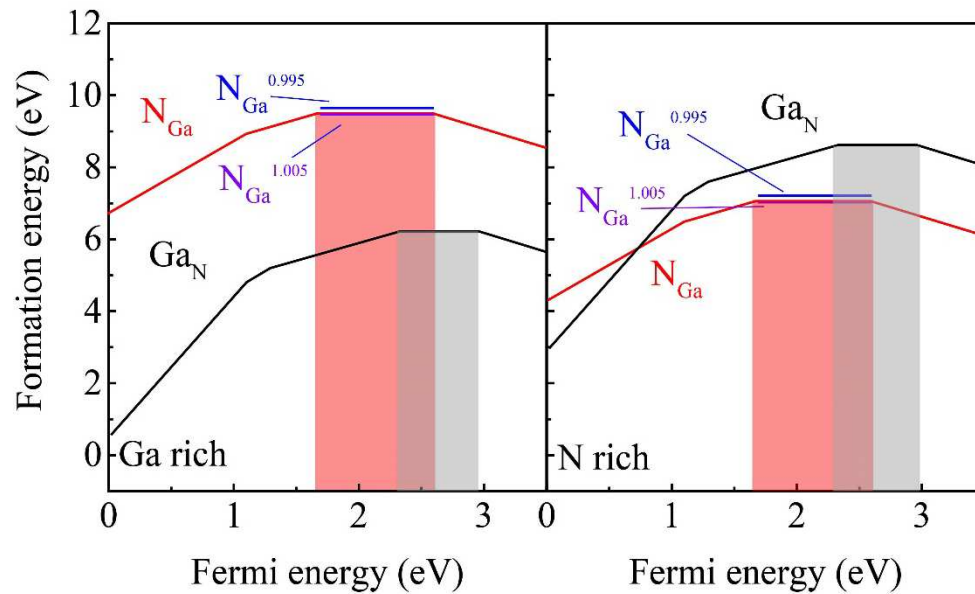


**Figure 2.** Formation energy of  $\text{GaN}$  and  $\text{N}_{\text{Ga}}$ , as a function of the Fermi level in N rich and Ga rich GaN. The zero and maximum of the Fermi-level scale corresponds to the top of the valence band and the bottom of the conduction band, respectively. The solid lines correspond to the formation energies for the most stable charge states of the defects. The  $\text{GaN}$  and  $\text{N}_{\text{Ga}}$  with  $\sigma = 1$  are present by black and red color. The  $\text{N}_{\text{Ga}}^{1.005}$  presented by blue and the  $\text{N}_{\text{Ga}}^{0.995}$  presented by purple are 0 state  $\text{N}_{\text{Ga}}$  with  $\sigma = 100.5\%$  and  $\sigma = 99.5\%$ .

### 3.2. Transition Channel and SPE Quality of Single-Atom Defects in GaN

Figure 3a illustrates the band structure of  $\text{GaN}^0$  and  $\text{N}_{\text{Ga}}^0$  with a strain of  $\sigma=1$ . For  $\text{GaN}^0$ , it is clear that the transition energy from to in the spin-down channel (0.5 eV) and the spin-up channel (0.6 eV) are both too small. Given that the zero-phonon line (ZPL) between those defect levels is typically even lower than the transition energy (usually half or less), the luminescence wavelength of  $\text{GaN}^0$  may exceed 4000 nm, which is far from telecommunication windows. On the other hand, for  $\text{N}_{\text{Ga}}$ , the highest occupied state  $a_1$  is isolated with a VBM of 0.3 eV, which avoids interference between defect levels and electronic states of the host material. The transition energy between  $a_1$  and  $a_2$  is 3 eV, which is large enough to avoid the influence of thermal excitations. These findings suggest that the defect levels of  $\text{N}_{\text{Ga}}^0$  could form a two-level system that satisfies SPE requirements. However, under additional strain, the defect level of  $\text{N}_{\text{Ga}}$  would be modified. The green and yellow arrows in Figure 3a represent the movement of defect levels when compressive and tensile stress is applied. When compressive strain is added,  $a_1$  and  $a_2$  ( $a_3$ ) move to a higher energy location, and the transition energy between  $a_1$  and  $a_2$  ( $a_3$ ) increases. Conversely, tensile strain causes the transition energy to decrease, and those defect levels move in the opposite direction. The specific numerical changes are shown in Table 1. Although defect levels  $a_1$  and  $a_2$  ( $a_3$ ) change by 0.2 eV as the strain changes from 100.5% to 99.5%, the transition energy between  $a_1$  and  $a_2$  ( $a_3$ ) remains almost unchanged (less than 0.03 eV). The effect of strain on  $\text{N}_{\text{Ga}}$  will be discussed in more detail in the next section.



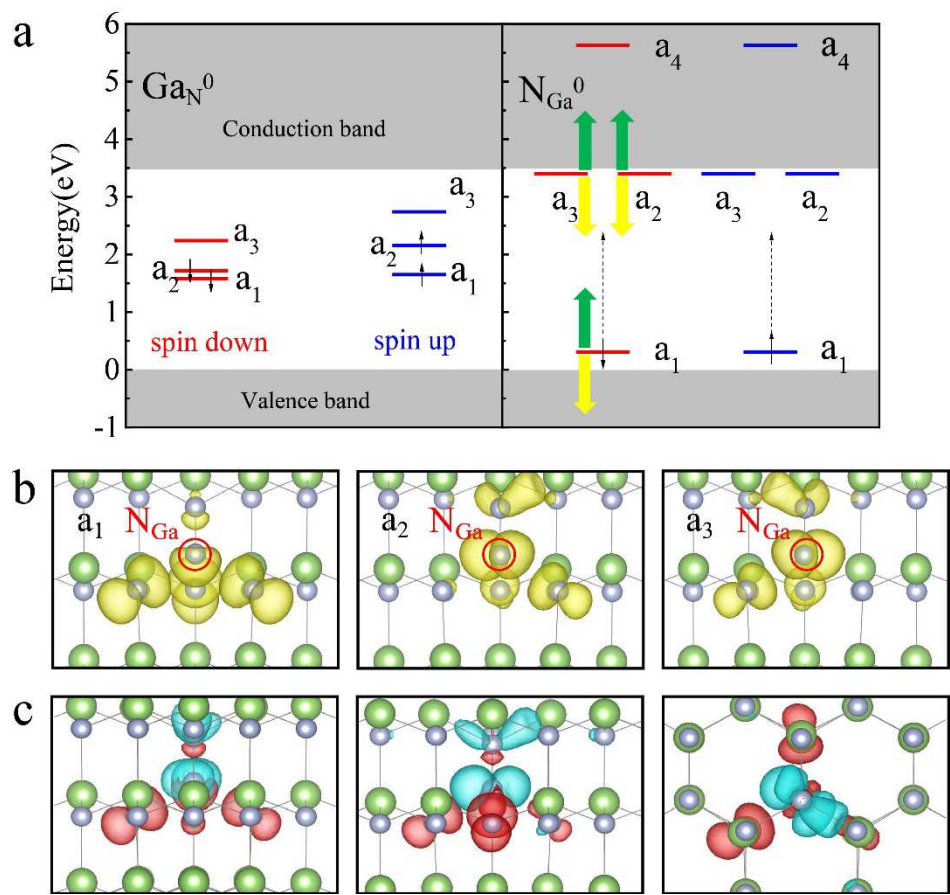


**Figure 3.** (a) band structure of GaN and N<sub>Ga</sub> with strain  $\sigma=1$ . The green and yellow arrow represents the movement of defect levels when the compressive stress and tensile strain is applied. The dashed arrows represent the transition channel. (b) the charge densities of  $a_1$ - $a_3$  of N<sub>Ga</sub>. (c)The front view, the side view, the top view of the charge density difference calculated by subtract the charge of  $a_2$  from  $a_1$ . The red and blue color represent positive and negative value.

**Table 1.** Location of defect levels of N<sub>Ga</sub> under different strain.

strain $\sigma$	99.5%	100%	100.5%
$a_1$ (eV)	0.459	0.334	0.224
$a_2$ (eV)	3.537	3.400	3.280
$a_2$ - $a_1$ (eV)	3.078	3.066	3.056

The charge densities of  $a_1$ - $a_3$  of N<sub>Ga</sub> at the gamma point are depicted in Figure 3b. These densities are mainly localized around the nitrogen substitution atom rather than being spread throughout the crystal. This suggests that the defect levels exhibit weak interaction with the host, which is advantageous for enhancing the purity of a SPE. Furthermore, the symmetry of the charge density of  $a_2$  and  $a_3$  is identical, indicating that these two defect levels are degenerate at the gamma point. Figure 3c displays the charge density difference obtained by subtracting the charge of  $a_2$  from that of  $a_1$ . The red and blue colors in the figure represent positive and negative values, respectively. As the electron transitions from  $a_1$  to  $a_2$ , the charge density progresses from the red part to the blue part. It is evident that the three nitrogen atoms, which are the second nearest neighbors of N<sub>Ga</sub>, primarily contribute to the red part. In contrast, the N<sub>Ga</sub> itself and the nitrogen atoms located at the upper nearest neighbor along the [0001] direction mainly contribute to the blue part. In other words, the charge density transfer during the transition occurs mainly from the second nearest neighbors of N<sub>Ga</sub> to both the N<sub>Ga</sub> itself and the nearest neighbor nitrogen. At  $a_2$ , one of the second nearest neighbor nitrogen atoms provides less charge than the other two due to the non-uniform distribution of charge density among these three atoms.

### 3.3. Defect Structure under Strain

Previous reports have proposed using strain to tune the luminescent properties of the defect single-photon emitter (SPE) in an effective way [12]. To analyze the geometry of the defect structure under strain, we calculated the bond length between atoms near  $N_{Ga}$ . Figure 4a,b shows the bond lengths between  $N_{Ga}$  and the nearest neighbor nitrogen atoms along the [0001] direction, as well as between the  $N_{Ga}$  and the second nearest neighbor nitrogen atoms. Table 1 summarizes the numerical changes in these bond lengths. Under triaxial compressive strain,  $d_1$  (the bond length between  $N_{Ga}$  and the upper nearest neighbor nitrogen atom) increases, while  $d_2$ - $d_4$  and  $d_5$ - $d_6$  (the bond lengths between  $N_{Ga}$  and the second nearest neighbor nitrogen atoms, and between the nearest neighbor nitrogen atoms and the second nearest neighbor nitrogen atoms) decrease. The opposite trend occurs under tensile strain. As discussed earlier, we know that the transition progress is realized primarily by transferring charge density from three second nearest neighbor nitrogen atoms to the  $N_{Ga}$  itself and the upper nearest neighbor nitrogen. The decrease in  $d_2$ - $d_4$  and  $d_5$ - $d_6$  under compressive strain promotes this process, leading to a lower ZPL. Conversely, the increase in these bonds under tensile strain leading to a higher the ZPL. Figure 4c,d shows the atom structure of  $N_{Ga}$  in the ground and excited states. We observe that the  $N_{Ga}$  in the excited state deviates noticeably from its original central position between the second nearest neighbor nitrogen atoms in the ground state. This deviation can be explained by the non-uniform charge transition in these three atoms from  $a_1$  to  $a_2$ .

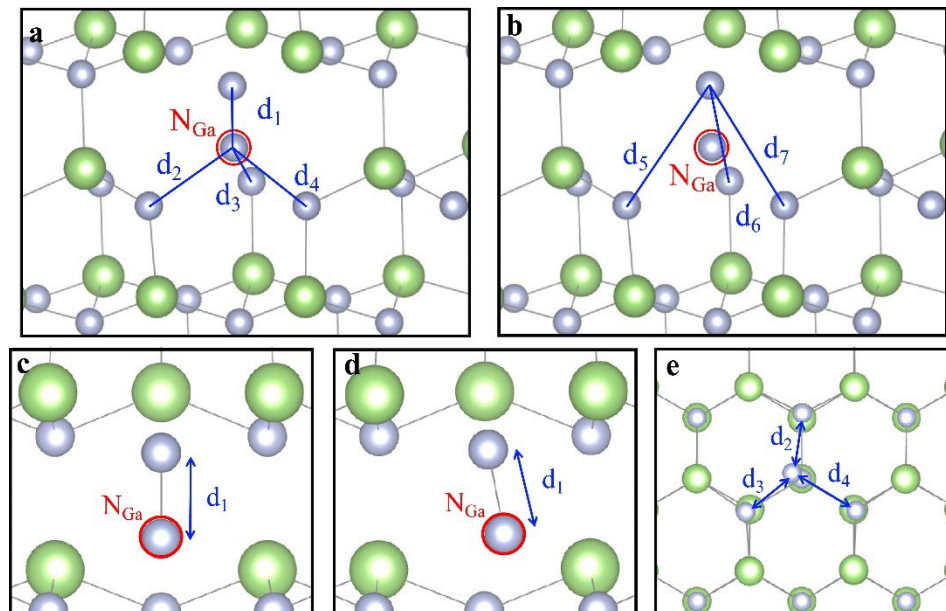


**Figure 4.** Structure diagram of  $N_{Ga}$  and bond length between atoms near  $N_{Ga}$ . (a,b) are the bond length between atoms near  $N_{Ga}$ . (c,d) are the side view of  $N_{Ga}$  in ground state and excited state. (e) is the top view of  $N_{Ga}$  in excited state.

**Table 2.** The bond distances of  $N_{Ga}$  under different strain.

state strain $\sigma$	ground state			excited state		
	99.5%	100%	100.5%	99.5%	100%	100.5%
$d_1$ (Å)	1.30316	1.28135	1.26637	1.31961	1.29306	1.27982
$d_2$ (Å)	2.97155	3.01326	3.05002	2.94662	3.02600	3.07573
$d_3$ (Å)	2.97246	3.01415	3.04992	3.03867	3.06722	3.10357
$d_4$ (Å)	2.97159	3.01335	3.05011	2.94824	3.02790	3.07888
$d_5$ (Å)	2.13592	2.18277	2.22577	2.02450	2.10169	2.15069
$d_6$ (Å)	2.13668	2.18351	2.22578	2.38010	2.45753	2.52477
$d_7$ (Å)	2.13595	2.18284	2.22584	2.02631	2.10348	2.15338

### 3.4. The Single Photon Emission Property under Strain

To evaluate the SPE performance of  $N_{Ga}$ , we calculated its ZPL and lifetime. Figure 5 shows the configuration coordinate diagram of the optical transition, where state 1 represents the ground state with an electron configuration of  $a_1^2 a_2^0$  and state 2 represents the excited state formed by exciting an electron from  $a_1$  to  $a_2$ . The photo absorption (PA) process involves an electron transition from the ground state to the excited state with the same configuration. The ZPL is the energy difference between the lowest energy of state 1 and 2. For  $N_{Ga}$  with a value of  $\sigma$  equal to 1, we calculated the PA and ZPL energies to be 1.01 eV ( $E_{PA}$ ) and 0.86 eV ( $E_{ZPL}$ ), respectively. The calculated PA energy of 1.01 eV suggests that the SPS can be excited by a near-infrared laser, such as the commercial 1064 nm laser. It's worth noting that the calculated ZPL energy of 0.86 eV (1442 nm) falls perfectly within the telecommunication windows.

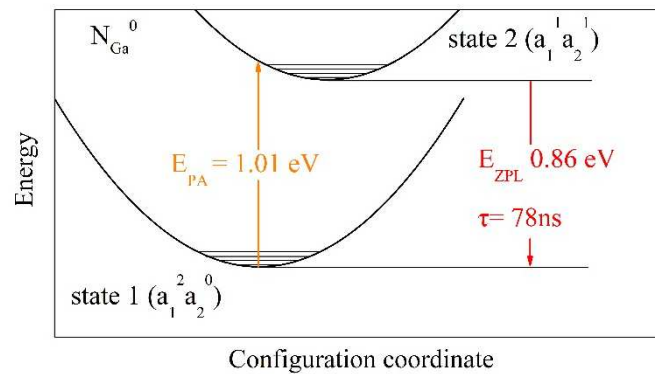


**Figure 5.** Configuration coordinate diagram of transition process between state 1 and state 2 in  $N_{Ga}$  without strain.

The radioactive lifetime  $\tau$  associated with ZPL can judge the quality of a SPE, which is given by  $\tau = \frac{1}{r_{ij}}$ . The transition rate  $r_{ij}$  can be given by Fermi's golden rule as:

$$r_{ij} = \frac{\omega^3 n |\mu_{ij}|^2}{3\pi\epsilon_0 \hbar c^3} \quad (2)$$

where  $\hbar$  is the reduced Planck constant,  $\omega$  is the frequency of the emitted photon of ZPL,  $|\mu_{ij}|$  is the transition dipole moment from state  $i$  to state  $j$ ,  $n$  is the refractive index,  $\epsilon_0$  is the vacuum permittivity, and  $c$  is the speed of light in vacuum, respectively. The transition channel in  $N_{Ga}$  could provide a two-level system, For  $N_{Ga}$  without strain, the calculated lifetime is 78 ns.

Table 3 shows that both the lifetime  $\tau$  and ZPL are affected when strain is applied. Specifically, the ZPL and lifetime exhibit a near-linear change with triaxial stress; lifetime increases with triaxial compressive strain, while ZPL decreases with an increase in triaxial compressive stress. The varying strain can modulate the ZPL from 0.849 eV (1460.5 nm) to 0.984 eV (1260 nm), covering the telecommunication windows from the O band to the E band. Moreover, the lifetime can be modulated from 86 ns to 18 ns. The reduction in ZPL with tensile strain is consistent with the previous discussions regarding charge density and bond. These results suggest that  $N_{Ga}$  under strain could meet the requirements for data transmission over optical fibers, and the lifetime could also be reduced to achieve an SPE with higher emission speed.

**Table 3.** The life time and ZPL of  $N_{Ga}$  under different strain.

Strain	99.5%	100%	100.5%
Life time $\tau$ (ns)	86.002	78.928	18.028
ZPL (eV)	0.84921	0.86482	0.98468



#### 4. Conclusion

We conducted a systematic investigation of the single photon emission properties of  $N_{Ga}$  in GaN under different triaxial strains using first-principles calculations. Our results demonstrate that  $N_{Ga}$  can serve as a bright and room-temperature single photon emitter. In particular, the addition of a triaxial strain can modulate the ZPL of  $N_{Ga}$  from 0.849 eV to 0.984 eV, covering the telecommunication windows from the O band to the E band, and the lifetime  $\tau$  from 18 ns to 86 ns. The calculated charge density and bond length suggest that the transition process is mainly affected by the distance from the  $N_{Ga}$  defect to its three second-nearest neighbor nitrogen atoms and its upper nearest-neighbor nitrogen. Our work sheds light on the possible origin of defect-based single photon emission in GaN and provides an effective method to achieve room-temperature single photon emission in the telecommunication windows.

**Acknowledgments:** The authors would like to acknowledge the financial support from National Natural Science Foundation of China No. 61704162, No. 11604227, 61704163, 11804239, NSAF U1830109, State Key Laboratory of Infrared Physics Open Project M201917 and Science Challenging Project No. TZ2016003.

#### References

1. A. Dietrich; M. W. Doherty; I. Aharonovich. Solid-state single photon source with Fourier transform limited lines at room temperature. *Phys. Rev. B*, 2020, 101, 081401.
2. M. A. Ortigoza; S. Stolbov. Thermodynamic stability and optical properties of C-doping-induced defects in hexagonal boron nitride as potential single-photon emitters. *Phys. Rev. B*, 2022, 105, 165306.
3. I. Aharonovich; D. Englund; M. Toth. Solid-state single-photon emitters. *Nat. Photonics*, 2016, 10, 631.
4. J. R. Weber; W. F. Koehl; J. B. Varley. Quantum computing with defects. *PANS*, 2010, 107, 8513.
5. X. Cao; M. Zopf; F. Ding. Telecom wavelength single photon sources. *Journal of Semiconductors*, 2019, 40, 071901.
6. M. A. P. Nguyen; J. Hite; M. A. Mastro, et al. Site control of quantum emitters in gallium nitride by polarity. *Appl. Phys. Lett.* 2021, 118, 021103.
7. S. G. Bishop; J. P. Hadden; R. Hekmati; J. K. Cannon; W. W. Langbein; and A. J. Bennett. Enhanced light collection from a gallium nitride color center using a near index-matched solid immersion lens. *Appl. Phys. Lett.* 2022, 120, 114001.
8. D. Li; K. Jiang; X. Sun; C. Guo. AlGaN photonics: recent advances in materials and ultraviolet devices. *Adv. Opt. Photonics* 2018, 10, 43.
9. A. M. Berhane; K.Y. Jeong; Z. Bodrog; S. Fiedler. Bright Room-Temperature Single Photon Emission from Defects in Gallium Nitride. *Adv. Mater.* 2017, 29, 1605092.
10. Y. Zhou; Z. Wang; A. Rasmita; S. Kim. Room temperature solid-state quantum emitters in the telecom range. *Sci. Adv.* 2018, 4, eaar3580.
11. H. Zang; X. Sun; K. Jiang. Cation Vacancy in Wide Bandgap III-Nitrides as Single-Photon Emitter: A First-Principles Investigation. *Adv. Sci.* 2021, 8, 2100100.
12. G. Grosso; H. Moon; B. Lienhard. Tunable and high-purity room temperature single-photon emission from atomic defects in hexagonal boron nitride. *Nature communications*, 2017, 8, 1-8.
13. J. Heyd; G.E. Scuseria; M. Ernzerhof. Hybrid functionals based on a screened Coulomb potential. *J. Chem. Phys.* 2003, 118, 8207.
14. W. Jia; J. Fu; Z. Cao; L. Wang; X. Chi; W. Gao; L.-W. Wang. Fast plane wave density functional theory molecular dynamics calculations on multi-GPU machines. *J. Comput. Phys.* 2013, 251, 102.
15. J. P. Perdew; K. Burke; M. Ernzerhof. Generalized gradient approximation made simple. *Phys. Rev. Lett.* 1996, 77, 3865.
16. D. O. Demchenko; I.C. Diallo; M.A. Reshchikov. Hydrogen-carbon complexes and the blue luminescence band in GaN. *J. Appl. Phys.* 2016, 119, 035702.
17. J. Yuan; Y. Hou; Z. Yang; F. Chen; Q. Li. GaN as a material platform for single-photon emitters: insights from ab initio study. *Adv. Opt. Mater.* 2022, 02158.
18. I. C. Diallo; D. O. Demchenko. Native Point Defects in GaN: A Hybrid-Functional Study. *Phys. Rev. Applied.* 2016, 6, 064002.
19. Z. Xie; Y. Sui; J. Buckeridge. Donor and acceptor characteristics of native point defects in GaN. *J. Phys. D: Appl. Phys.* 2019, 52, 335104.
20. A. Kyrtsos; M. Matsubara; E. Bellotti. Migration mechanisms and diffusion barriers of carbon and native point defects in GaN. *Phys. Rev. B* 2016, 93, 245201.
21. 18.Z. Suo; J. Luo; S. Li; L. Wang. Image charge interaction correction in charged-defect calculation. *Phys. Rev. B* 2020, 102, 174110.